Vibrational Analysis of Metalloporphyrins with Electron-Withdrawing NO_2 Substituents at Different Meso Positions

Christina Lemke,[‡] Reinhard Schweitzer-Stenner,*[,§] John A. Shelnutt,[||] J. Martin E. Quirke,[⊥] and Wolfgang Dreybrodt[‡]

Institut für Experimentelle Physik, Universität Bremen, 28359 Bremen, Germany, Department of Chemistry, University of Puerto Rico, Río Piedras Campus, P.O. Box 23346, San Juan, Puerto Rico 00931, Biomolecular Materials and Interfaces Department, Sandia National Laboratories, Albuquerque, New Mexico 87815-1349, Department of Chemistry, The University of New Mexico, Albuquerque, New Mexico 87131, and Department of Chemistry, Florida International University, Miami, Florida 33199

Received: March 27, 2001

The structure of metalloporphyrins is to a major extent determined by its peripheral substituents. To explore the influence of NO_2 meso substituents, we have measured polarized resonance Raman spectra of Ni(II)(5-NO_2−octaethylporphyrin) and Ni(II)(5,15-NO_2−octaethylporphyrin) at various excitation wavelengths in the Soret and Q band region in CS_2. We obtained very complex and overcrowded spectra that were self-consistently analyzed by a global fitting procedure. This revealed that numerous Raman lines in the Raman frequency region are composed of sublines. This includes all prominent structural marker lines. Thus, we found that for both substances at least three conformers coexist in solution. The resonance excitation profiles of the corresponding sublines indicate that these conformers exhibit different degrees of nonplanarity. Altogether, the data suggest that the nitro groups destabilize the porphyrin macrocycle and increase conformational heterogeneity. We also performed a normal-mode calculation with a spectroscopically determined molecular mechanics force field for a nonplanar structure of Ni(II)(5,15-NO_2−octaethylporphyrin). This revealed that the NO_2 substituents lower the symmetry of some vibrations by vibrational mixing (e.g., for ν_4) and by changing the eigenvectors in particular of low-frequency modes (e.g., of ν_8).

Introduction

Over the last 20 years, the influence of peripheral substituents on the structure and physicochemical properties of metalloporphyrins has become a major subject of research.[1−3] In crude terms, two different groups of substituents can be distinguished.[2,3] The first one comprises bulky alkyl and aryl substituents attached to the meso and β carbons. Steric interaction between these substituents generally gives rise to sometimes-significant nonplanar distortions, which can mostly be described as a superposition of saddling, ruffling, and, to some extent, waving.[3−5] The second group contains substituents with a strong electron-withdrawing capacity such as NO_2 or simple halogens such as Cl or Br.[2,6] These cause an electron-deficient macrocycle, which may serve as a convenient acceptor in electron-transfer chains.[7] To use electron-withdrawing substituents in an effective way for porphyrin design, one needs to study in detail their influence on the structure, function, and electronic properties of porphyrin macrocycles. In this context, it is also important to investigate how these substituents may affect structural distortions imposed by the steric interaction between substituents. To this end, it is necessary to study metalloporphyrins with mixed alkyl(aryl) and electron-withdrawing substituents.[8]

In the present study, we use resonance Raman spectroscopy to investigate the properties of two nitro-substituted Ni(II)−octaethylporphyrins, namely, the meso substituted Ni(II)-5-NO_2-2,3,7,8,12,13,17,18−octaethylporphyrin [Ni(5-NO_2−OEP)] and Ni(II)-5,15-NO_2-2,3,7,8,12,13,17,18−octaethylporphyrin [Ni-(5,15-NO_2−OEP)] (Figure 1). These and related substances (e.g., the fully substituted Ni(5,10,15,20-NO_2−OEP and its free base analogue) have already been investigated by resonance Raman, optical, and NMR spectroscopy,[9,10] time-resolved fluorescence spectroscopy,[11] and X-ray crystallography.[12] The results indicate that the nitro substitution destabilizes the porphyrin macrocycle with respect to nonplanar distortions. The Raman data and the molecular mechanics calculations suggest the possible coexistence of multiple conformers. However, the analysis of the Raman spectra in the studies by Anderson et al.[9] and Hobbs et al.[10] were only based on spectra taken at a single excitation wavelength. In the case of coexisting conformers, which contribute overlapping lines to the spectra, this may not be sufficient basis for a detailed analysis. In the present study, we have measured polarized Raman spectra of the above nitroporphyrins at numerous wavelengths covering the entire B and Q band region. These spectra were subjected to a global self-consistent fit to obtain and distinguish even heavily overlapping Raman lines. From these data, we obtained the resonance excitation profiles (REPs) and depolarization ratio dispersions (DPD) of all identified Raman lines. All these data provide evidence that at least three different conformers of Ni(5-NO_2−OEP) and Ni(5,15-NO_2−OEP) coexist in CS_2. Finally, we have carried out a normal coordinate calculation by employing a slightly modified version of a force field that we recently obtained for Ni(II)−octaethylporphyrin.[13] Thus, it is shown for

* Corresponding author. Tel. 787-764-0000 (ext. 2417). Fax: 787-756-8242. E-mail: rstenner_upr_chemistry@gmx.net.
[‡] Universität Bremen.
[§] University of Puerto Rico.
[||] Sandia National Laboratories and The University of New Mexico.
[⊥] Florida International University.

10.1021/jp011137u CCC: $20.00
Published on Web 06/13/2001

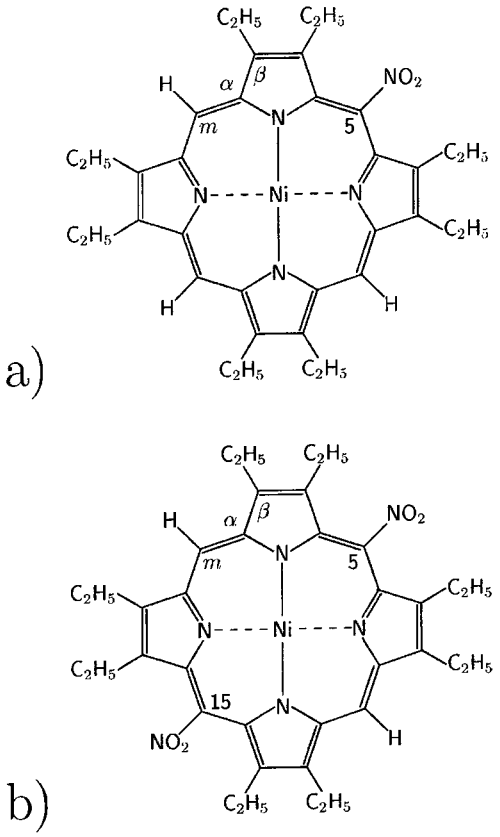

Figure 1. Structures of (a) Ni(5-NO_2−OEP) and (b) Ni(5,15-NO_2−OEP).

the first time how asymmetric substituents affect eigenvectors of porphyrin vibrations. The nonplanar distortions of the conformers are investigated in more detail by polarized resonance Raman dispersion spectroscopy. This study was reported in the previous paper of this issue.[14]

Material and Methods

Preparation. The nitroporphyrins Ni(II)-5-NO_2−octaethylporphyrin [Ni(5-NO_2−OEP)] and Ni(II) 5,15-NO_2−octaethylporphyrin [Ni(5,15-NO_2−OEP)] were prepared by employing the method of Bonnett and Stephenson.[15] The purity required for UV−vis and Raman spectroscopy was checked by thin-layer chromatography using Kieselgel with fluorescence indicator F254 (Merck).

UV−Vis Absorption and Resonance Ramam Spectroscopy. All substances were dissolved in CS_2 (Aldrich, HPLC grade) up to concentrations of about 0.5 mM. UV−vis spectra were recorded by a two-beam spectrometer (Shimadzu UV-2101PC) using a quartz cell with an optical pathway of 1 mm.

The resonance Raman spectra were measured using an excimer pumped dye laser system and a cw laser system to give higher spectral resolution, both described in detail elsewhere.[16] A cylindrical lens was used to focus the laser beam on the sample. The line focus was oriented parallel to the spectrometer's entrance slit. We used a backscattering geometry with a polarization analyzer followed by a scrambler between collimator and the entrance slit of the spectrometer to measure the Raman intensity of the two components polarized parallel (I_x) and perpendicular (I_y) to the scattering plane. To avoid local heating, we placed the sample in a rotating quartz cell (50 Hz). The REPs and DPDs were obtained by using the dye laser system to measure polarized Raman spectra of Ni(5-NO_2−OEP) and Ni(5,15-NO_2−OEP) with excitation wavelengths between 380 and 580 nm. The spectra were taken every 2 nm in resonance and every 4 nm off resonance. Thus, the observed data cover the Q_0, Q_v, and B resonance regions. The corrections for the transfer functions of the spectrometers and for self-absorption and the calibration of the spectra were carried out as described by Unger et al.[16] The strong 656 cm^{-1} band of CS_2 was used as an internal standard for determining the intensities of the porphyrin Raman bands.

The experimentally observed depolarization ratio $\rho = I_y/I_x$ is affected by the solid angle of the collimator, which images the scattering volume of the sample onto the entrance slit of the spectrometer.[17] If the porphyrin exhibits D_{4h} symmetry, one therefore observes depolarization ratios of 15, 0.15, and 0.77 instead of the theoretical values ∞, 0.125, and 0.75, respectively.

Curve Fitting. To identify the frequency positions, line profiles, and line widths (full widths at half-maximum = fwhm) of all Raman lines, we employed our line-shape analysis program called MULTIFIT. The Raman lines were fitted with a convolution of a line profile (Lorentzian or Gaussian) and the spectrometers transfer function. We eliminated ambiguities in the line shape analysis by using the same frequency, half-width, and line shape to fit each Raman line for all excitation wavelengths. Thus, we obtained a self-consistent global fit of about 80 spectra, for which only the line intensities were used as free fitting parameters. We worked on small spectral regions to minimize the number of free parameters in the fitting procedure. It is important to choose the regions carefully so that overlapping lines are fitted simultaneously to perform a reliable analysis of of the respective Raman spectra. The background intensity was accounted for by a linear function or a second-order polynomial. For the first identification of the Raman line parameters, we used the Raman spectra measured with cw lasers because they could be recorded with better spectral resolution. By comparison of Raman spectra measured with the (pulsed) excimer pumped dye and a cw-laser using the same excitation wavelengths, we further identified Raman lines of excited electronic states[18] induced by the high power density of the dye laser pulses. The Raman half-widths given in the tables are true widths corrected for the spectrometers transfer functions. The integrated band intensities obtained from the spectral analysis were finally used to determine the REPs and DPDs of a large number of Raman lines.

Normal Coordinate Analysis. The normal coordinate analysis of Ni(5-NO_2−OEP) and Ni(5,15-NO_2−OEP) was carried out by employing the method developed by Unger et al.[13,19] These authors used a 6−12 Lennard Jones potential to describe noncovalent interactions. In the present study, we used instead a 6−9 potential in order to reduce the interaction of local coordinates separated by three or a larger number of bonds. This was rendered necessary because calculations with the 6−12 potential yielded nitro groups oriented perpendicular to the porphyrin plane. It is known, however, that as a substituent of cyclic hydrocarbons, the nitro group is always twisted out-of plane by about 40°.[20] We assumed a similar orientation for porphyrin substituent.

The initial force constants for the two nitroporphyrins were taken from the recently obtained reduced force field of NiOEP[13] and that of nitrobenzol. The ethyl groups were oriented alternating above and below the porphyrin macrocycle. The optimization of the force field was carried out by employing an iterative self-consisten procedure. First, we optimized the molecular structure using the above force field. Subsequently,

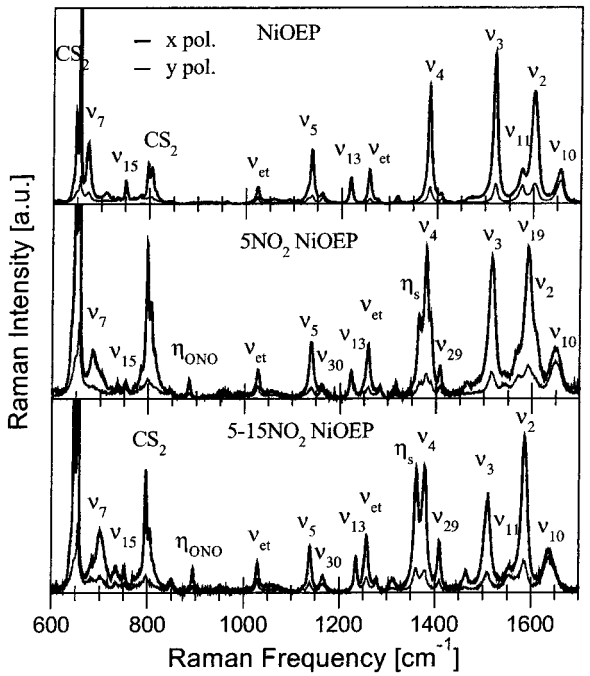

Figure 2. Resonance Raman spectra of NiOEP (406.7 nm), Ni(5,15-NO_2−OEP) (413 nm), and Ni(5-NO_2−OEP) (413 nm) measured with Soret band excitation.

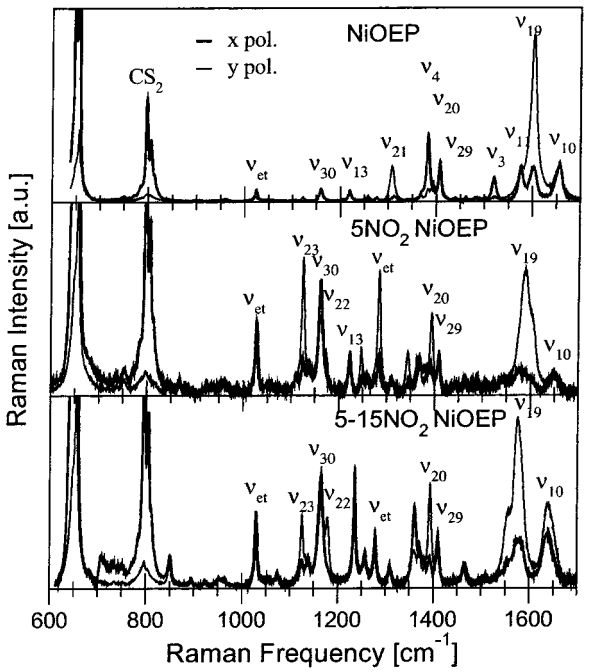

Figure 3. Resonance Raman spectra of NiOEP (514.5 nm), Ni(5,15-NO_2−OEP) (530.0 nm), and Ni(5-NO_2−OEP) (530.9 nm) measured with Q_v band excitation.

we performed a normal coordinate calculation to obtain the frequencies of the normal modes. Optimization was then carried out by varying the force constants to minimize the difference between theoretically and experimentally obtained frequencies. For those lines which are composed of two or three sublines, we always used the highest-frequency subline, which, as we will show below, always corresponds to a conformer with the lowest degree of nonplanar distortion. The thus obtained refined force field was employed to obtain a new optimized structure, for which we recalculated the normal-mode frequencies. The procedure was repeated until convergence was obtained.

Results

Raman Spectra. Figures 2−4 display representative polarized Raman spectra of NiOEP [6], Ni(5-NO_2−OEP), and Ni(5,-15NO_2−OEP) in CS_2 between 600 and 1700 cm^{-1} with excitation wavelengths in the B, Q_v, and Q_0 band, respectively. The most prominent bands in the respective spectra are labeled using the nomenclature that Li et al.[21] employed for NiOEP. Apparently, the spectra of the asymmetrically nitro-substituted porphyrins are more complex than those of the symmetrically substituted NiOEP. The spectra of all nitro-substituted porphyrins depict a line assignable to the symmetric (η_s) NO_2 stretching mode. In addition, the spectra of Ni(5-NO_2−OEP) show a line resulting from the antisymmetric NO_2 stretching mode (η_a). These modes get resonance-enhanced with B as well as with Q band excitation. Finally, the spectra of Ni(5-NO_2−OEP) exhibit Raman lines from modes having E_u symmetry in D_{4h}, which become Raman active due to the asymmetric perturbation caused by the nitro groups.

Spectral Analysis. By employing the protocol described under Materials and Methods, we performed a detailed spectral analysis of the polarized resonance Raman spectra of the above nitro-substituted porphyrins. Figures 5−8 depict the decomposition of the particularly overcrowded spectral regions between 1450 and 1700 as well as between 1330 and 1430 cm^{-1} for Ni(5-NO_2−OEP) (Figures 5 and 6) and Ni(5,15-NO_2−OEP)

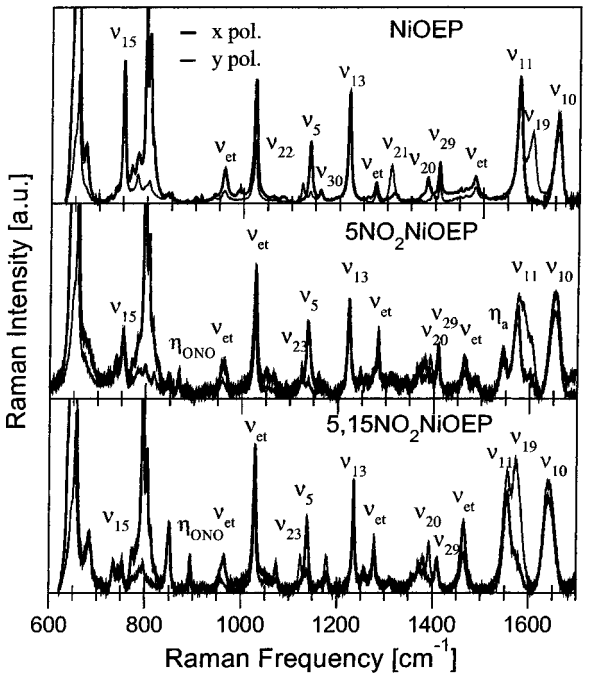

Figure 4. Resonance Raman spectra of NiOEP, Ni(5,15-NO_2−OEP) (568.2 nm), and Ni(5-NO_2−OEP) measured with Q_0 band (568.2 nm) excitation.

(Figures 7 and 8). The spectral parameters of all Raman lines identified above 600 cm^{-1} are listed in Table 1. Raman lines arising from a photoexcited state of the central Ni(II) atom are marked by an asterisk.

Figure 9 compares the polarized Raman spectra measured with a CW krypton laser and the pulsed excimer pumped dye laser at the same excitation wavelength. The additional lines in the spectra observed with pulsed laser excitation are indicated in the figures. They are assignable to a photoexcited state which involves a d−d transition of the Ni(II) atom.[18] The accuracy of our spectral analysis enabled us to obtain REPs even of this

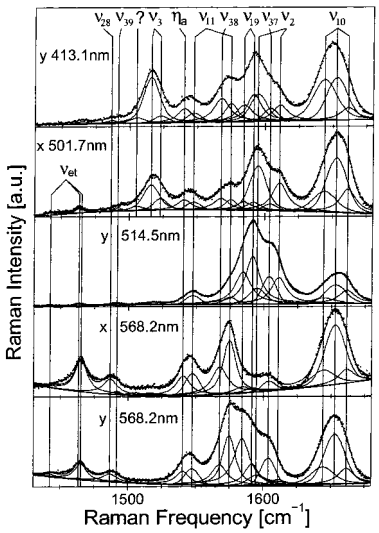

Figure 5. Ni(5-NO_2−OEP): Spectral decomposition of the fingerprint region for different excitation wavelengths and polarization directions (*x*, parallel; *y*, perpendicular to the incident polarization).

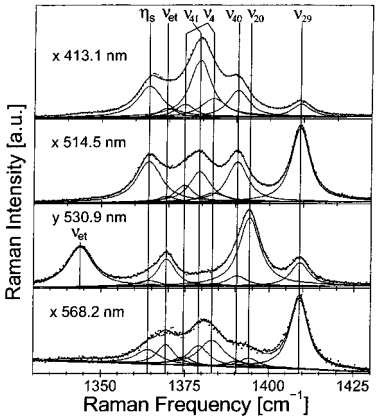

Figure 6. Ni(5-NO_2−OEP): Spectral decomposition of the ν_4 spectral region for different excitation wavelengths and polarization directions (*x*, parallel; *y*, perpendicular to the incident polarization).

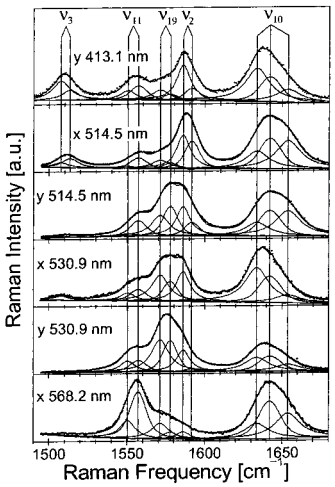

Figure 7. Ni(5,15-NO_2−OEP): Spectral decomposition of the fingerprint region for different excitation wavelengths and polarization directions (*x*, parallel; *y*, perpendicular to the incident polarization).

photoexcited Raman lines. Details will be given in a separate publication (Lemke et al. Manuscript in preparation).

Assignment of Ni(5,15-NO_2−OEP) Lines. The vibrational analysis was first done for Ni(5,15-NO_2−OEP) because it has the highest symmetry of the nitro-substituted porphyrins investigated. For the assignment of the experimentally observed Raman lines to porphyrin modes, we made use of the known assignments for NiOEP[13,21] and NiOETPP.[13,22,23] Moreover, the respective REPs and DPDs were utilized in order to distinguish between modes of different symmetry. In D_{4h}, A_{1g} (B_{1g}, B_{2g}), and A_{2g}, modes exhibit constant depolarization ratios of 0.125, 0.75, and ∞, respectively. In the presence of symmetry-lowering distortions, the depolarization ratio depends on the excitation wavelength. However, its deviation from the D_{4h} value is modest in some wavelength region (e.g., the Soret band region for A_{1g}-type modes) so that the original depolarization ratio can still be identified.[24] Moreover, REPs can be used to some extent to distinguish Raman lines from modes of different symmetry. This holds in particular for B_{1g}- and B_{2g}-type modes, since the former is always more intense with Q_0 than with Q_v excitation while the latter shows exactly the opposite behavior.[25]

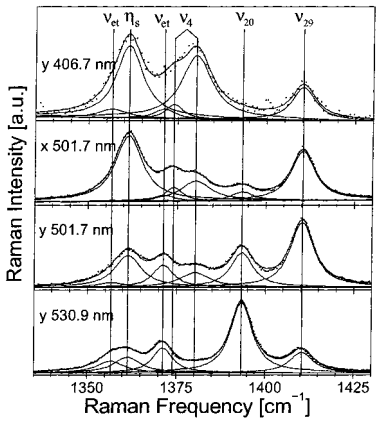

Figure 8. Ni(5,15-NO_2−OEP): Spectral decomposition of the ν_4 spectral region for different excitation wavelengths and polarization directions (*x*, parallel; *y*, perpendicular to the incident polarization).

The Raman spectra of Ni(5,15-NO_2−OEP) exhibit some similarity with those of NiOEP (cf. Figures 2−4). Therefore, the assignment of the Raman lines to the normal modes is straightforward (Table 1). In the fingerprint region above 1500 cm^{-1}, the classical structure sensitive lines appear at 1640 cm^{-1} (ν_{10}), 1587 cm^{-1} (ν_2), 1573 cm^{-1} (ν_{19}), 1554 cm^{-1} (ν_{11}), and 1510 cm^{-1} (ν_3) (Figure 7). ν_{10} can be decomposed into three sublines, while two sublines could be inferred from the remaining marker lines. This is indicative of coexisting conformers which exhibit different degrees of nonplanarity.[16,26] The next spectral region between 1430 and 1470 cm^{-1} displays only some weak lines resulting from asymmetric deformation[2] and scissoring modes[15] of the ethyl substituents.

Between 1300 and 1430 cm^{-1}, the macrocycle vibrations ν_{29} (1410 cm^{-1}), ν_{20} (1393 cm^{-1}), a ν_4-doublet (1380 and 1374 cm^{-1}), and two bands resulting from ethyl vibrations (1371 and 1357 cm^{-1}) were identified. Additionally, we obtained the symmetric NO_2 stretch η_s at 1361 cm^{-1}, which is strongly resonance-enhanced with B band excitation and still exhibits a detectable enhancement in the Q band region (cf. the REP in Figure 11). It seems that in contrast to NiOEP, ν_4 also appears as a doublet at 1380 and 1374 cm^{-1}. Because of results from a normal coordinate analysis of propane,[16] the lines at 1371, 1357, and 1316 cm^{-1} are assignable to symmetric deformation and wagging modes of the ethyl substituents. Similar to spectra of other metalloporphyrins, ν_{21} appears at 1310 cm^{-1}.[21]

Interestingly, several lines in the region between 1300 and 1100 cm^{-1} are also underlied by two sublines, namely, ν_{22}, ν_{30}, and ν_5 at 1179, 1164, and 1137 cm^{-1}. ν_{13} appears as a single

TABLE 1: Spectral Parameters Obtained from an Analysis of the Raman Spectra of Ni(5-NO_2−OEP) and Ni(5,15-NO_2−OEP)[a]

mode	sym. type	Ni(5-NO_2−OEP)	Γ_L, cm^{-1}	Γ_G, cm^{-1}	Ni(5,15-NO_2−OEP)	Γ_L, cm^{-1}	Γ_G, cm^{-1}
		605.0	3.3	19.3	–		
		631.2	14.0	–	–		
CS_2		639.6	5.9	–	–		
		–			640.1	4.2	–
CS_2		647.6	3.8	1.7	647.0	2.3	3.9
CS_2		–			652.3	0.8	–
CS_2		653.4	3.3	–	653.7	1.4	–
CS_2		656.0	0.3	1.9	656.0	0.4	2.4
		673.0	5.7	–	660.5	4.6	–
		–			684.9	14.0	–
ν_7^{LF}	Λ_{1g}	681.6	7.3	–	–		
ν_7^{HF}	A_{1g}	686.9	7.4	–	700.9	12.4	–
		695.0	10.3	–	–		
		705.4	10.9	–	708.1	13.7	–
		721.8	3.0	–	–		
		735.4	3.4	–	732.3	5.9	–
		738.8	6.4	–	736.2	6.3	–
		746.3	4.6	–	745.1	6.0	–
ν_{15}^{LF}	B_{1g}	751.8	6.5	–	749.2	5.7	–
ν_{15}^{HF}	B_{1g}	755.8	6.9	–	754.3	4.8	–
	A_{1g}	771.7	6.7	–	–		
		–			774.8	5.4	–
	A_{1g}	778.8	5.4	–	783.9	7.1	–
		784.3	6.3	–	–		
	B_{1g}	789.5	6.9	–	–		
		–			790.4	6.2	–
CS_2		796.8	4.7	–	797.1	4.3	–
		799.4	6.5	–	–		
CS_2		805.8	4.7	–	805.9	5.5	–
CS_2		813.2	4.7	–	813.6	5.0	–
		817.1	6.7	–	–		
		–			820.3	3.6	–
		825.1	9.8	–	–		
		844.8	6.4	–	848.0	6.8	–
		850.7	7.0	–	852.0	6.0	–
		868.5	3.7	–	–		
O−N−O	A_{1g}	884.0	6.2	–	–		
O−N−O	A_{1g}	885.5	5.0	–	895.4	4.6	–
	A_{2g}	923.7	7.2	–	922.8	7.5	–
ν_{32}^{LF}	B_{2g}	933.1	7.7	–	–		
ν_{32}^{HF}	B_{2g}	950.7	8.6	–	951.0	8.9	–
		–			957.7	11.7	–
	B_{1g}	959.1	9.0	–	–		
	A_{1g}	965.2	8.0	–	–		
		–			966.2	8.4	–
		–			989.1	5.9	–
	B_{2g}	1003.9	6.0	–	–		
		1021.5	6.1	–	–		
		1026.8	6.3	–	–		
		1029.1	5.3	–	–		
ν_{et}	B_{1g}	–			1029.8	6.4	–
	B_{1g}	1049.8	8.6	–	–		
ν_{et}	A_{1g}	1056.8	8.6	–	1057.4	15.0	–
		1065.8	6.3	–			
		1067.7	8.5	–			
ν_{et}	A_{1g}	–			1074.5	6.5	–
ν_{44}	Eu	1109.6	5.7	–	–		
ν_{23}	A_{2g}	1124.5	7.0	–	1125.4	6.7	–
ν_{14}	B_{1g}	1132.4	5.2	–	–		
ν_5^{LF}	A_{1g}	1137.2	7.3	–	1135.6	6.7	–
ν_5^{HF}	A_{1g}	1140.2	8.0	–	1139.7	6.5	–
ν_{43}	Eu	1145.9	6.4	–	–		
ν_{30}^{LF}	B_{2g}	1161.8	10.0	–	1162.1	10.6	–
ν_{30}^{HF}	B_{2g}	–			1166.7	9.9	–

TABLE 1 (Continued)

mode	sym. type	Ni(5-NO_2−OEP)	Γ_L, cm^{-1}	Γ_G, cm^{-1}	Ni(5,15-NO_2−OEP)	Γ_L, cm^{-1}	Γ_G, cm^{-1}
ν_{22}^{LF}	A_{2g}	1173.0	8.4	−	1178.2	7.5	−
ν_{22}^{HF}	A_{2g}	−			1180.7	7.2	−
ν_{13}^{*}	B_{1g}	1216.0	5.0	−	−		
ν_{13}^{LF}	B_{1g}	1222.6	5.8	−	−		
ν_{13}^{HF}	B_{1g}	1228.5	5.3	−	1235.7	6.1	−
ν_{42}	*Eu*	1246.3	5.9	−	−		
ν_{et}	B_{2g}	−			1252.5	7.7	−
ν_{et}	A_{1g}	1256.6	7.9	−	1257.5	6.6	−
ν_{et}	A_{2g}	1260.1	6.8	−	1260.4	8.2	−
ν_{et}	B_{1g}	1274.5	9.6	−	1278.7	7.4	−
ν_{et}	A_{2g}	1283.4	6.3	−	−		−
–21	A_{2g}	1307.3	4.8	−	1309.6	6.4	−
ν_{et}	B_{2g}	1311.1	5.3	−	−		
ν_{et}	A_{1g}	1316.4	6.7	−	1316.0	5.8	−
ν_{et}	A_{1g}/A_{2g}	1343.8	8.7	−	1356.6	8.8	−
η_s	A_{1g}	1364.0	8.3	−	1361.3	8.6	−
ν_{et}	A_{1g}/A_{2g}	1369.3	5.8	−	1371.2	6.4	−
ν_{4}^{LF}	A_{1g}	1374.5	6.4	−	1373.9	5.1	−
ν_{41}	*Eu*	1379.1	7.1	−	−		
ν_{4}^{HF}	A_{1g}	1383.1	8.9	−	1380.1	10.0	−
ν_{40}	*Eu*	1390.4	6.9	−	−		
ν_{20}^{*}	A_{2g}	−			1389.1	7.0	−
ν_{20}	A_{2g}	1394.1	7.0	−	1393.3	7.0	−
ν_{29}	B_{2g}	1409.0	5.9	−	1410.3	7.4	−
ν_{et}^{*}	A_{2g}	−			1438.8	4.1	−
ν_{et}	A_{2g}	1442.3	10.9	−	1444.5	8.9	−
ν_{et}	A_{2g}	1463.4	6.0	−	1463.9	8.6	−
ν_{et}	A_{1g}	1465.2	10.0	−	1468.2	9.5	−
ν_{28}	B_{2g}	1486.7	12.5	−	−		
ν_{39}	*Eu*	1491.7	7.2	−	−		
$\nu_{6+7/13+17}$	A_{1g}	1505.3	13.2	−	−		
ν_{3}^{LF}	A_{1g}	1516.1	7.1	9.9	1507.6	13.5	−
ν_{3}^{HF}	A_{1g}	1522.9	4.7	9.4	1513.3	12.2	−
η_a	B_{1g}	1540.4	12.6	−	−		
ν_{11}^{*}	B_{1g}	−			1535.3	15.3	−
ν_{11}^{LF}	B_{1g}	1547.3	2.2	11.3	1550.3	11.7	−
ν_{38}	*Eu*	1567.7	13.9	−	−		
ν_{11}^{HF}	B_{1g}	1574.8	8.7	5.4	1557.1	7.8	7.9
ν_{19}^{*}	A_{2g}	1578.0	10.0	−	−		
ν_{19}^{LF}	A_{2g}	1584.4	14.0	−	1571.1	13.4	−
ν_{19}^{HF}	A_{2g}	1591.5	12.4	−	1577.6	6.2	7.6
ν_{2}^{LF}	A_{1g}	1594.8	6.8	10.8	1585.9	10.5	−
ν_{37}	*Eu*	1603.7	0.6	12.3	−		
ν_{2}^{HF}	A_{1g}	1610.9	13.4	−	1591.5	7.0	7.1
ν_{10}^{*}	B_{1g}	1631.0	8.5	10.0	1623.9	13.1	−
ν_{10}^{LF}	B_{1g}	1644.0	8.5	15.8	1633.6	18.5	−
ν_{10}^{MF}	B_{1g}	1652.9	3.6	16.4	1642.0	8.0	12.3
ν_{10}^{HF}	B_{1g}	1661.4	14.3	−	1653.6	19.5	−

[a] The basis for the assignments is described in the text. The type of symmetry given assumes D_{4h} symmetry. Γ represents the fwhm of the Lorentzian or Gaussian profiles. The asterisk * indicates those bands which result from photoinduced enhancement.

line at 1236 cm^{-1}. Minor contributions in this spectral region stem from other ethyl twisting modes and from the ν_{23} at 1125 cm^{-1}.

In the frequency region between 600 and 1000 cm^{-1} we mostly observed Raman lines of low intensity that stem mainly from ethyl vibrations. Calculations show symmetric stretch modes at 900 cm^{-1} and rocking modes at 760 cm^{-1}. As the intensity is not large enough to provide us with a sufficiently good DPD to identify their symmetry type, we did not assign those lines. Nevertheless, we identified the Raman lines of the porphyrin modes ν_{32}, ν_{15}, and the ν_7, a number of CS_2 modes and the O−N−O bending vibration. Additionally, we tentatively assign the weak lines observed at 708 and 735 cm^{-1} to the out-of-plane modes γ_5 (A_{2u}) and γ_{15} (B_{2u}), in line with results from the normal coordinate calculation.

We also measured the low-frequency region between 200 and 500 cm^{-1} with 413 nm excitation (data not shown). Besides ν_8 and ν_9, we identified some lines resulting from B_{2u}- and A_{2u}-type out-of-plane vibrations (e.g., γ_{16} at 251 cm^{-1} and γ_6 at 351 cm^{-1}). ν_8 appears very broad with a Gaussian half-width of 27 cm^{-1}, indicating that it is composed of subbands that cannot be resolved by a single experiment. Such a heterogeneity was earlier obtained for NiOEP[26] and NiTPP (Ni(II)−tetraphenylporphyrin).[16]

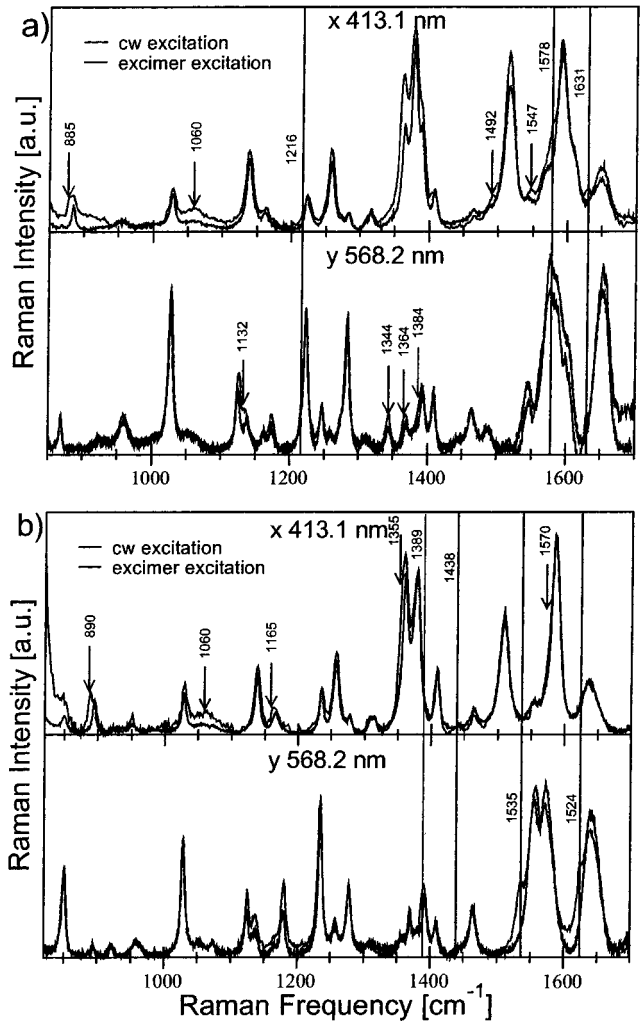

Figure 9. Identification of photoinduced Raman lines in the spectra of (a) Ni(5-NO_2−OEP) and (b) Ni(5,15-NO_2−OEP) by comparison of spectra obtained by CW and pulsed excitation as described in the text.

Assignment of Ni(5-NO_2−OEP) Lines. A complete assignment of all lines observed from the spectral analysis is given in Table 1. The spectra recorded between 1700 and 1500 cm^{-1} appear more complex compared with Ni(5,15-NO_2−OEP) because E_u-type modes become Raman-active due to the symmetry-lowering perturbation of the NO_2 group (Figures 2−4). For their respective assignment, we used results from our normal coordinate calculation and information from NiOEP IR spectra (data not shown). They appear at 1604 cm^{-1} (ν_{37}) and 1568 cm^{-1} (ν_{38}). As observed for Ni(5,15-NO_2−OEP), ν_{10} (at 1653 cm^{-1}) contains three sublines, while the remaining marker modes (ν_2, ν_{19}, ν_3, ν_{11}) exhibit two. Interestingly, the splitting between some of the corresponding sublines is much more pronounced than that in the spectra of Ni(5,15-NO_2−OEP). ν_2, for instance, shows a split of 16 cm^{-1} compared with 6 cm^{-1} obtained for Ni(5,15-NO_2−OEP). This indicates that the either the structural difference between the conformers is quantitatively more pronounced for Ni(5-NO_2−OEP) or the two conformers of the latter are composed of different nonplanar deformations, which has a different impact on the frequencies of the structure sensitive modes. Different frequency sensitivities were shown by Franco et al. et al. for a series of ruffled porphyrins and a series of saddled porphyrins.[27] A line arising from η_a was observed at 1540 cm^{-1}.

As usual, the region between 1400 and 1500 cm^{-1} contains only some comparatively weak lines resulting from B_{2g}, E_u, and ethyl vibrations. Between 1300 and 1400 cm^{-1}, the spectra of both NO_2-porphyrins investigated are comparable in that ν_4 also appears as a doublet and η_s as a strongly enhanced line, especially with B band excitation (Figure 2). As one expects, some additional lines from E_u-type modes appear between 1100 and 1400 cm^{-1}. A remarkable difference with respect to Ni(5,15-NO_2−OEP) is that even ν_{13}, which is generally not a very structure sensitive band, appears with two sublines at 1223 and 1229 cm^{-1}. This again indicates that the structural difference between the corresponding conformers is very pronounced.

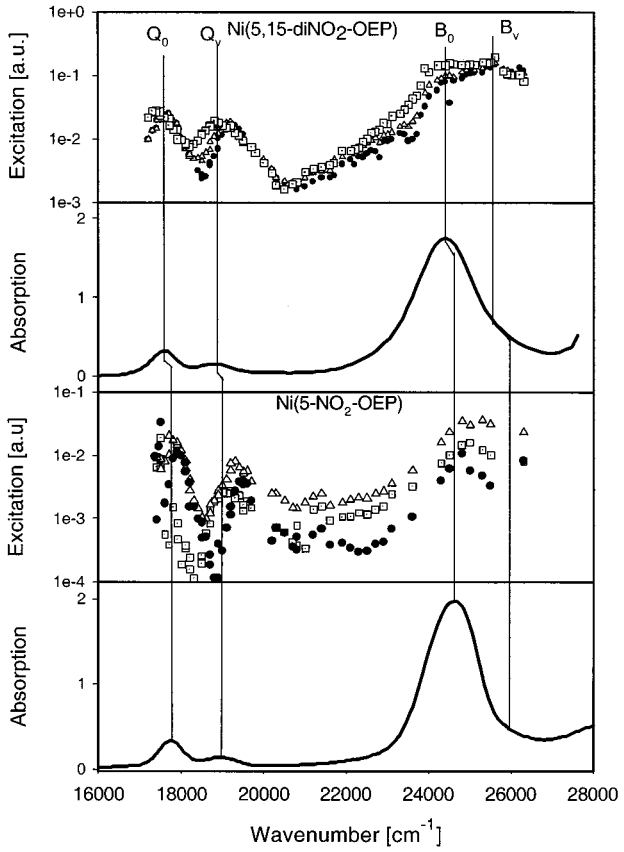

Figure 10. REPs of the ν_{10} sublines of (a) Ni(5-NO_2−OEP) and (b) Ni(5,15-NO_2−OEP).

Below 1100 cm^{-1}, we again identified the Raman lines ν_{32}, ν_{15}, and ν_7, the O−N−O vibration, some CS_2 lines, and a number of ethyl modes.

In the low-frequency spectrum between 200 and 500 nm, we again identified ν_8, ν_9 and some lines from out-of-plane distortions (data not shown).

Resonance Excitation Profiles. As mentioned above, various Raman lines of 5,15- and Ni(5-NO_2−OEP) can be decomposed into two or even three sublines. Our spectral analysis enabled us to obtain the REPs of all the sublines in the Ni(5,15-NO_2−OEP) spectra with high precision. Thus, we found that with the exception of ν_{15} and ν_{30}, the REP of the respective lower frequency subline is redshifted with respect to the higher-frequency subline. As an example, Figure 10 compares the REPs of the sublines of ν_{10}. The magnitude of the red shift observed for the remaining low-frequency sublines are listed in Table 2.

For Ni(5-NO_2−OEP), the strong overlap between various bands did not allow us to determine the REPs of sublines with the same accuracy as that for Ni(5,15-NO_2−OEP). However, red shifts for low-frequency sublines could unambiguously be obtained for ν_2, ν_3, ν_7, ν_{10}, ν_{13}, and ν_{19}. The REPs of the ν_{10} sublines for Ni(5-NO_2−OEP) are also shown as an example in

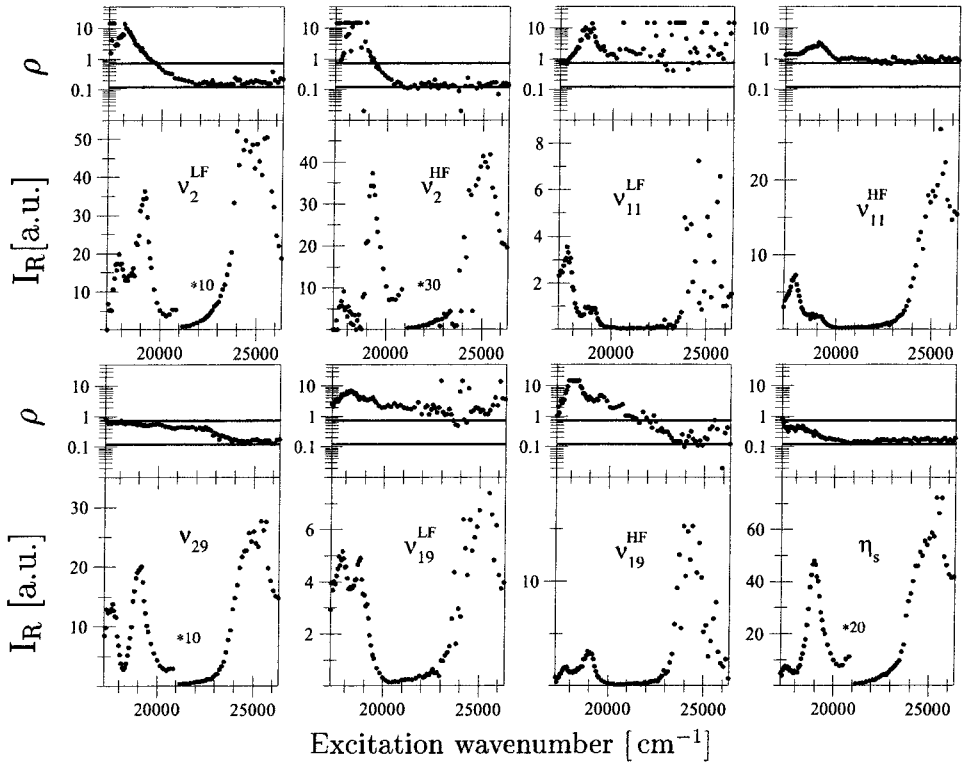

Figure 11. DPDs and REPs of the ν_2, ν_{11}, ν_{29}, ν_{19}, and η_s modes of Ni(5,15-NO_2−OEP).

TABLE 2: Ni(5,15-NO_2−OEP): Red-shift of the REPs of Lower-Frequency Sublines as Obtained for the Indicated Raman Lines[a]

normal mode	Q_0 [cm^{-1}]	Q_v [cm^{-1}]	B [cm^{-1}]
		150	
ν_2			
ν_3		230	
ν_{10}^{LF-MF}	220	195	250
ν_{10}^{MF-HF}	120	140	280
ν_{11}	140	140	
ν_{19}	77	160	

[a] The data have a relative error of 30%.

Figure 10. The sublines of ν_{15} and ν_{32} do not show any red shift.

Figure 11 depicts the REPs of the Raman lines from ν_2, ν_{11}, ν_{29}, and ν_{19} of Ni(5,15-NO_2−OEP), which represent the four different symmetry types A_{1g}, B_{1g}, B_{2g}, and A_{2g}, respectively. Additionally, the REP of η_s is shown to demonstrate the strong resonance enhancement of its Raman line. As usual, the A_{1g} modes exhibit the largest intensity with Soret excitation, while the asymmetric modes are predominantly enhanced with Q_0 and Q_v excitation. As observed earlier for other metal porphyrins, the Raman lines arising from B_{1g}-type modes exhibit a strong Q_0 enhancement, which is much larger than that predicted by Gouterman's four orbital model.[24,25] The REPs of the remaining lines identified above 1000 cm^{-1} are given in the Supplementary Information. Some of them were analyzed together with the corresponding DPR dispersion data. Results obtained from this study are presented in the subsequent paper.[14]

Depolarization Ratios. We have measured the DPDs of all Raman lines of both substances investigated. Nearly all of them exhibit a strong DPR dispersion, which is indicative of significant symmetry-lowering perturbations caused by the nitro substituents. As an example, Figure 11 depicts the DPDs of the representative modes ν_2, ν_{11}, ν_{29}, and ν_{19}. The DPDs of the remaining lines identified above 1000 cm^{-1} is given in Supplementary Information. A thorough theoretical analysis of some of these data sets, from which a detailed picture of the symmetry lowering distortions was obtained, is described in detail in the subsequent paper.[14]

TABLE 3: Wavelengths of the Absorption Maxima of NiOEP,[26] Ni(5-NO_2−OEP), Ni(5,15-NO_2−OEP), NidiPrP,[5] NiTPP,[29] and NiOETPP[22] in CS_2

porphyrin	B [nm]	Q_v [nm]	Q_0 [nm]
NiOEP	406	524	558
5-NO_2NiOEP	406	528	564
5,15-NO_2NiOEP	410	532	568
nidiPrP	418	531	559
NiTPP	424	531	562
NiOETPP	446	560	596

Absorption Spectra. Table 3 compares the wavelength positions of the absorption maxima of Ni(5-NO_2−OEP) and Ni(5,15-NO_2−OEP) with those earlier observed for NiOEP,[26] Ni(II)-5,15-di-iso-propylporphyrin (NiDiPrP), Ni(II)-4,10,15,-20-tetraphenylporphyrin (NiTPP)[16], and NiOETPP.[28] Both nitroporphyrins show absorption maxima which are red-shifted with respect to NiOEP and comparable with those of NiDiPrP and NiTPP. As observed earlier, the absorption spectrum of NiOETPP exhibits the most pronounced redshift.[28]

Normal Coordinate Analysis. We have performed a combined molecular mechanics/normal coordinate calculation of Ni(5-NO_2−OEP) and Ni(5,15-NO_2−OEP) as described in Material and Methods. To this end, we assumed that the ethyl substituents exhibit a $\alpha\beta\alpha\beta\alpha\beta\alpha\beta$ configuration. As we show elsewhere, this is only one of many possible nearly isoenergetic ethyl configurations. While conformers with different ethyl orientations may exhibit different nonplanar distortions, the differences in normal-mode composition and frequencies, at least of the high-frequency modes, are certainly smaller so that the conformer with the above configuration can be considered as representative.

TABLE 4: Experimental Frequencies of the Structural Sensitive Normal Modes of NiOEP, Ni(5-NO_2−OEP), Ni(5,15-NO_2−OEP), and NiOETPP[a]

PED[x]	ν_i	NiOEP	5-NO_2NiOEP	5-NO_2NiOEP*
$C_\beta-C_\beta(45)$	ν_2	1602−1608	1595−1611	1589
$C_\beta-C_\beta(70)$	ν_{11}	1576	1547−1575	
$C_\beta-C_\beta(28)$, $C_\alpha-C_m(28)$	ν_3	1518−1521	1516−1523	1513
$C_\alpha-C_m(83)$	ν_{10}	1652−1658	1644−1661	1644−1654
$C_\alpha-C_m(88)$	ν_{19}	1598−1604	1584−1592	
PED[x]	ν_i	5,15-NO_2 NiOEP	5,15-NO2 NiOEP*	NiOETPP
$C_\beta-C_\beta(45)$	ν_2	1586−1592	1585	1563
$C_\beta-C_\beta(70)$	ν_{11}	1550−1557		1509
$C_\beta-C_\beta(28)$, $C_\alpha-C_m(28)$	ν_3	1508−1513	1509	1504
$C_\alpha-C_m(83)$	ν_{10}	1634−1654	1636	−
$C_\alpha-C_m(88)$	ν_{19}	1571−1578		1490

[a] The specified frequency ranges are determined by the lowest- and the highest-frequency sublines. The left column lists the local coordinates with the largest contribution to the potential energy distribution (PED). The experimental data were taken from Li et al.,[21] Unger[325] (NiOEP), Hobbs et al.[10] (5-NO_2-NiOEP* and 5,15-NO_2-NiOEP*), and Stichternath et al.[22] (NiOETPP).

The results of the calculations are listed in Tables 4 and 5. Table 4 provides the predominant contributions to the potential energy distribution (PED) to the structure sensitive modes. The experimentally and theoretically calculated frequencies are given in Table 5. Table 6 lists some structural parameters which emerged from the optimization procedure which yielded some B_{1u}-type ruffling (reflected by the twist angle) with a slight admixture of saddling (i.e., the angle N−Ni−N differs from 180°). Apparently, the degree of nonplanarity increases with the number of nitro substituents, in agreement with our experimental data. Compared with earlier molecular mechanics calculations by Hobbs et al.,[10] we underestimate ruffling by a factor of 3, while our saddling distortion is slightly larger.

In particular in the low-frequency region, it was not possible to make a complete assignment to Raman lines due to the limited information obtainable from the low-frequency spectra (Figure 5). In the high-frequency region above 1100 cm^{-1}, the frequency of the observed Raman lines could be reproduced with satisfactory accuracy.

Figure 12 exhibits the eigenvectors of some representative in-plane vibrations of Ni(5,15-NO_2−OEP) of different D_{4h} symmetries, namely, the A_{1g} modes ν_2, ν_3, ν_4, and ν_8, the B_{1g} modes ν_{10}, ν_{11}, and ν_{18}, the B_{2g} modes ν_{29} and ν_{34}, and the A_{2g} modes ν_{19} and ν_{21} and also the eigenvectors of the nitro modes η_s and η_a. The eigenvectors of some low frequency out-of-plane modes are shown in Figure 13.

Discussion

Raman and Absorption Spectra. The structural sensitivity of the "core size marker lines" ν_2, ν_3, ν_{10}, ν_{11}, and ν_{19} has been exploited in numerous studies to explore structural changes imposed by axial ligand binding and interactions between the porphyrin and its (protein) environment. While Spiro and coworkers[29] provided much evidence for a linear correlation between the macrocycle core size and the frequencies of the above modes, Shelnutt and associates[28,30] found that the latter are also affected by nonplanar distortions; i.e., the more nonplanar the porphyrin, the lower the frequency of the marker lines. That notion holds in particular for ruffling distortions.[31]

Earlier resonance Raman studies showed that two conformers of the classical-model porphyrin NiOEP coexist in various organic solvents.[26] They can be distinguished in that they give rise to different sublines for the above structural marker lines. The high-frequency sublines were assigned to a nearly planar conformer, while the respective low-frequency sublines were interpreted to result from a nonplanar, ruffled conformer. Furthermore, experimental[32] and theoretical[14] evidence suggest that both populations are still heterogeneous in that they consist of different subconformers with different ethyl orientations. Table 4 compares the subline frequencies of the two nitroporphyrins investigated with those of NiOEP and NiOETPP. Apparently, the high-frequency sublines of Ni(5-NO_2−OEP) are very close to those of the planar conformer of NiOEP, whereas the corresponding low frequency sublines appear at much lower frequencies than their NiOEP counterparts. Only ν_{19} departs from this rule; its high-frequency subline (1592 cm^{-1}) is at a significantly lower frequency than observed for NiOEP (1604 and 1598 cm^{-1}). Bearing in mind the strong $C_\alpha-C_m$ contribution to the PED of the ν_{19} (cf. Table 4), one may relate this shift to a direct influence of the electron-withdrawing nitro substituents, and therefore, it does not necessarily suggest a nonplanar deformation. Hence, one might suspect that the high-frequency sublines of Ni(5-NO_2−OEP) result from a conformer which is comparable to the planar NiOEP conformer, whereas the lower-frequency sublines stem from a conformer which is significantly more nonplanar than that observed for NiOEP in solution. However, as we will discuss below and in more detail in another paper,[14] the DPD data of the sublines clearly show that all detectable conformers are nonplanar due to the coexistence of ruffling and saddling distortions.

It should be mentioned that Hobbs et al.[10] have assigned the Raman line at 1589 cm^{-1} to ν_2, while our line-shape analysis revealed overlapping bands in this spectral region. The corresponding DPDs suggest that the two components of ν_2 are at higher frequencies, i.e., at 1595 and 1611 cm^{-1}, whereas a line at 1591 cm^{-1} is assignable to the high-frequency subline of ν_{19}. For ν_{10}, the authors observed only two sublines at 1644 and 1654 cm^{-1}, while our analysis yielded three sublines at 1644, 1653, and 1661 cm^{-1}.

All sublines of Ni(5,15-NO_2−OEP) are more redshifted than those of Ni(5-NO_2−OEP), which, in agreement with expectation, points to a higher degree of nonplanarity. With respect to NiOETPP,[22,30] all sublines of the nitro porphyrins are at higher frequencies, suggesting that the latter are less nonplanar than the former. However, as shown by resonance Raman dispersion spectroscopy in the subsequent paper,[14] the information solely obtained from the observed frequency shifts of the marker lines do not provide a complete picture of the structural difference between the porphyrins compared above, because different types of nonplanar distortions have a significantly different influence on the frequencies of the marker lines.

The analysis of ν_{10} reveals the existence of at least three coexisting conformers, whereas only two sublines were obtained

TABLE 5: Comparison of Experimental and Calculated Frequencies of in-plane Normal Modes of NiOEP,[31] NiTPP,[16] Ni(5-NO_2−OEP), and Ni(5,15-NO_2−OEP)[a]

	NiOEP		NiTPP		Ni(5-NO_2)		Ni(5,15-NO_2)	
ν [cm^{-1}]	obs.	calcd	obs.	calcd	obs.	calcd	obs.	calcd
				A_{1g}				
1		3054	1235	1228		3051		
2	1602	1612	1572	1569	1611	1593	1592	1591
3	1520	1505	1470	1470	1523	1493	1513	1491
4	1383	1360	1374	1382	1383	1388	1380	1389
5	1138	1126		3055	1140	1172	1140	1175
		1188						
6	804	776	1004	983		823		827
		826						
7	676	664	889	896	687	687	701	731
8	350	341	395	391		342		376
9	270	273	1078	1089		320		318
				B_{1g}				
10	1655	1654	1600	1597	1661	1635	1654	1636
11	1577	1572	1504	1505	1575	1553	1557	1550
12		1380	1302	1304		1378		1370
13	1220	1284	238	242	1229	1259	1236	1219
14	1131	1136		3055	1132	1121		1118
		1192						
15	751	765	1015	1005	756	800	754	810
16	740	740	846	850		749		753
17	305	287	277	266		242		204
18	168	193	1084	1081		188		188
				A_{2g}				
19	1603	1610	1550	1552	1592	1597	1578	1600
20	1393	1393	1341	1339	1394	1400	1393	1400
21	1307	1303		279	1307	1276	1310	1270
22	1121	1109	1016	1013	1173	1094	1181	1198
23	1058	1064		3052		1060	1125	1058
24	597	584	828	801		608		624
25	551	533	560	550		523		525
26		279	1230	1226		258		265
				B_{2g}				
27		3053	1269	1284		3050		3051
28	1483	1495	1485	1479	1487	1503		1503
29	1407	1388	1377	1384	1409	1412	1410	1411
30	1159	1092		1057	1162	1191	1167	1204
		1199						
31	1015	998		3053		1044		1109
		1017						
32	?938	662	869	888	951	1017	951	1051
33	493	525	450	463		666		668
34	197	219	1190	1179		167		152
35	144	169	109	109		128		124
				Eu				
37		1634			1604	1621		1624
38		1588			1568	1568		1566
39		1486			1492	1495		1495
40		1411			1390	1408		1408
41		1368			1379	1381		1368
42		1275			1246	1269		1269
43		1133			1146	1164		1164
44		1080			1110	1112		1116

[a] The normal modes were calculated for conformations with alternating ethyl orientations.

for the remaining marker modes. This means that one of the respective sublines must be considered as an overlap of two sublines that cannot be distinguished. In principle, this discrepancy is not surprising, because ν_{10} is the most sensitive structural marker mode. Moreover, all high-frequency sublines were fitted by Voigtian profiles with a significant Gaussian contribution. This points to further structural heterogeneity.

For all marker lines, the REPs of the lower frequency sublines are redshifted with respect to those of the high frequency components (Figure 10 and Table 2). This is expected for conformers exhibiting a different degree of nonplanarity. As suggested by experimental and theoretical studies, nonplanar distortions usually give rise to a red shift of the $0 \rightarrow 0$ energies of the transitions into the Q and B states, which also determine the energy of maximal resonance enhancement. Thus, reds-hifted REPs are assignable to conformers with larger nonplanar distortions. Those sublines for which the REPs do not show any detectable red shift may be assigned to conformers with different ethyl orientations or of different types of nonplanar distortions that do not cause red shifts.

TABLE 6: Structural Parameters of NiOEP (Unger, Personal Communication), Ni(5-NO_2−OEP), and Ni(5,15-NO_2−OEP) from a Molecular Mechanics Calculations with a Spectroscopically Determined Force Field[a]

	NiOEP	5-NO_2NiOEP	5,15-NO_2NiOEP
"core size" [Å]	2.0497	2.0484	2.0510
N−Ni−N [deg]	179.85	179.50	179.13
C_α−N_1-C_α [deg]	106.98	108.26	108.20
C_α−N_2-C_α [deg]	106.92	108.25	108.11
C_α−N_3-C_α [deg]	107.03	107.99	108.11
C_α−N_4-C_α [deg]	106.98	108.05	108.21
C_α−N_{m5}-C_α [deg]	127.04	123.65	123.32
C_α−N_{m10}-C_α [deg]	127.08	124.41	124.80
C_α−N_{m15}-C_α [deg]	126.97	123.73	123.40
C_α−N_{m20}-C_α [deg]	126.99	124.42	124.88
"twist angle" [deg]	0.53	2.30	4.14

[a] "Core size", Ni−N distance; "twist angle", torsion of opposite pyrroles with respect to each other).

The absorption spectra provide essentially the same information as the Raman data. As shown in numerous papers by Shelnutt and co-workers,[28,30] nonplanar distortions usually cause a red shift of the entire absorption spectrum. The data in Table 3 reveal that Ni(5-NO_2−OEP) and Ni(5,15-NO_2−OEP) range between NiOEP and NiOETPP, comparable with NiTPP and NiDiPrP. However, one has to consider that the nitro groups cause a blueshift of the absorption spectrum due to their $\pi\pi$ interaction with the A_{2u} and E_g orbitals, but it is unlikely that this accounts for the 30 nm difference between the spectra of NiOETPP and Ni(5,15-NO_2−OEP).

Taken together, the Raman spectra of Ni(5-NO_2−OEP) and Ni(5,15-NO_2−OEP) suggest the coexistence of at least three conformers with different degrees of nonplanarity. A comparison with spectra of NiOEP and NiOETPP suggest that at least all conformers of Ni(5,15-NO_2−OEP) are nonplanar but less distorted than NiOETPP. Overall, the data show that the nitro groups destabilize the structure of the porphyrin macrocycle.

Symmetry-Lowering Distortions. In principle, the NO_2 substituents of the two porphyrins investigated give rise to perturbations which lower the macrocycle symmetry of Ni(5-NO_2−OEP) and Ni(5,15-NO_2−OEP) from D_{4h} to $C_{2v}(C_2')$ and $D_{2h}(C_2'')$, respectively. Following Gouterman,[33] one can describe the symmetry-lowering also in terms of distortions classified by the irreducible representations of the D_{4h} point group. Thus, one obtains a B_{2g} in-plane distortion for Ni(5,15-NO_2−OEP), while Ni(5-NO_2−OEP) is subject to B_{2g} and E_u in-plane distortions. The latter give rise to the Raman activity of E_u modes.

This group theoretical consideration does not allow any prediction of the strength of the imposed symmetry perturbation nor to any sterically induced out-of-plane deformations.. The DPDs of the Raman lines as shown in Figure 11 and in the supplementary information, however, indicate to a very strong influence of the nitro substituents. The dispersion is caused by mixing vibronic coupling contributions of different symmetry

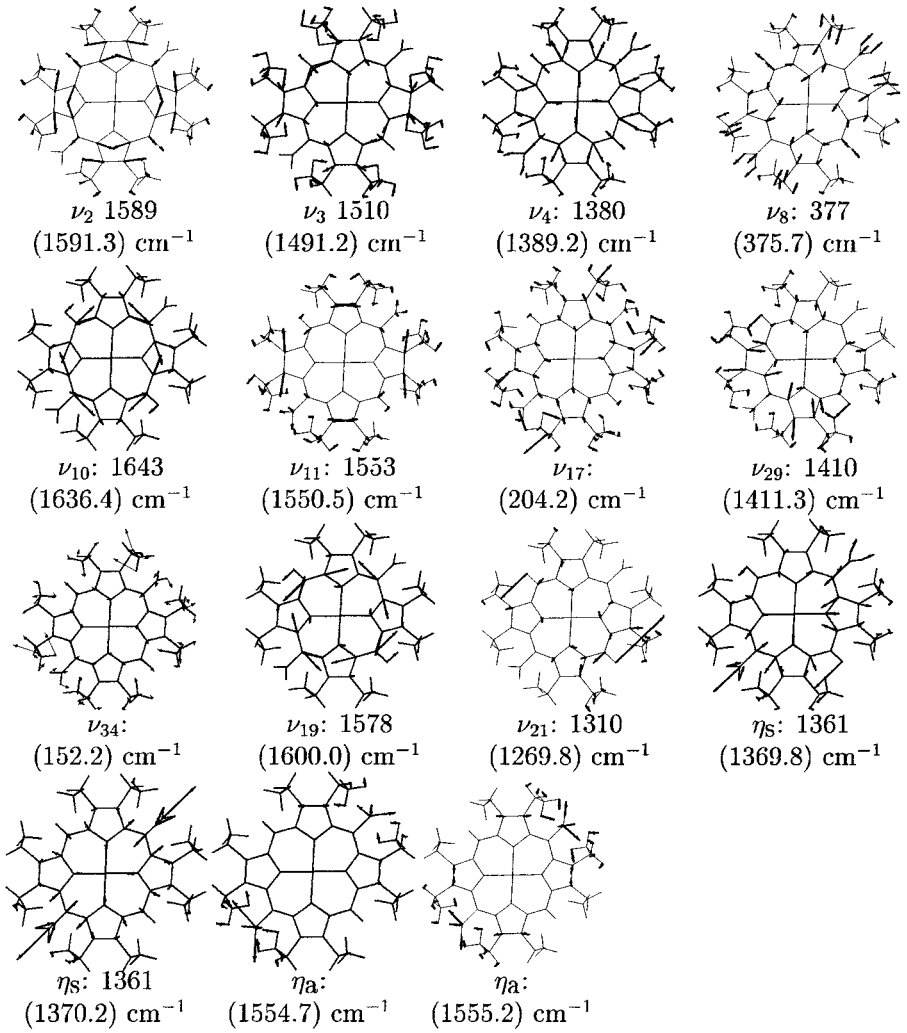

Figure 12. Eigenvectors of a representative set of normal vibrations of Ni(5,15-NO_2−OEP) calculated as described in Material and Methods.

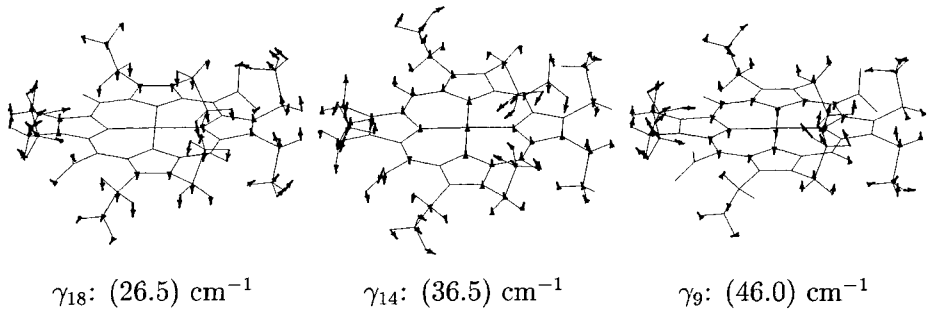

Figure 13. Eigenvectors of the low-frequency out-of-plane modes γ_{18} (B_{2u}, saddling), γ_{14} (B_{1u}, ruffling), and γ_9 (A_{2u}, doming).

into the Raman tensor.[34] In the case of a B_{2g} distortion, theoretical considerations outlined elsewhere[34] show that the depolarization ratios of A_{1g} and B_{2g} modes are supposed to vary between 0.125 and 0.75, while those of B_{1g} and A_{2g} modes should exhibit values between 0.75 and ∞. The DPDs shown in Figure 11 are in accordance with this prediction for ν_{11} and ν_{29}, whereas the DPDs of the other Raman lines (ν_2, ν_{19}) exhibit an even stronger dispersion, which, as discussed in refs 14 and 34, can be rationalized in terms of the presence of nonplanar distortions.

It should be emphasized that the changes of the depolarization ratio shown in Figure 11 are large compared with corresponding DPDs measured for porphyrins embedded in heme proteins,[35] where the symmetry of the macrocycle is lowered by asymmetric peripheral substituents and even more by the protein environment. This is indicative of an exceptionally strong influence of the nitro groups on the porphyrin macrocycle.

Normal Coordinate Analysis. The eigenvectors shown in Figure 12 reveal two possible influences of the NO_2 groups on the normal-mode pattern. First, it is possible that internally the NO_2 interacts with local modes of the porphyrin to yield a normal vibration that is delocalized over the macrocycle and the NO_2 substituents. Good examples are the normal modes of ν_4, ν_8, ν_{11}, ν_{18}, and ν_{34}. Second, the electronic influence of the nitro groups (electron-withdrawing and $\pi\pi$ interaction) have an impact on the force constants so that the symmetry of the macrocycle vibration is directly affected. An excellent example is ν_3. In NiOEP, this mode is mostly a $C_\alpha C_m$ stretch with some

ethyl contributions.[21] In Ni(5,15-NO_2−OEP), the $C_\alpha C_m$ contributions adjacent to the NO_2 substituents are nearly eliminated, but they are still present at the unsubstituted meso carbons (Figure 12). Thus, the mode actually transforms like the representation A_g in the D_{2h} point group (if one neglects nonplanarity). Another even more compelling example is ν_8. In NiOEP, this mode can be described as an in-phase motion of the pyrrole rings[21] along the N−Ni−N lines. In Ni(5,15-NO_2−OEP), however, the pyrrole motions are heavily perturbed, and the internal symmetry of the pyrrole ring is no longer maintained. A similar effect though somewhat less pronounced was obtained for ν_7 and ν_9 (data not shown). This shows that the influence of the NO_2 groups is not limited to the adjacent methine bridges. The electronic interaction with the macrocycle perturbs the entire structure and affects in particular the normal-mode pattern for in-plane low-frequency modes.

The out-of-plane vibrations shown in Figure 13 are relevant for the structural deformability of porphyrins in that out-plane-distortions can predominantly be represented as a superposition of these eigenvectors.[4] γ_9 (A_{2u}) is the classical doming mode which is of high importance for the dynamics of heme groups.[36] γ_{14} (B_{1u}) is a ruffling coordinate whereas the saddling distortion is mostly represented by γ_{18} (B_{2u}).

Summary

This study presents a very detailed spectral analysis of the Raman spectra of the two nitroporphyrins Ni(5-NO_2−OEP) and Ni(5,15-NO_2−OEP). We showed that for both substances at least three different conformers coexist in solution and that they exhibit a different degree of nonplanarity. Furthermore, we found that the asymmetric substitution of the NO_2 groups have a major impact of the symmetry of some normal modes by (1) vibrational coupling between NO_2 and porphyrin vibrations and (2) by changing the eigenvector composition in particular of some low frequency modes which mainly involve the pyrrole groups. A strong asymmetric perturbation of the macrocycle is also indicated by the exceptional depolarization ratio dispersion of all Raman lines investigated. This is analyzed in detail in the subsequent paper.[14]

Acknowledgment. Part of this project was supported by the European Community in the Framework of the network program "The Dynamics of Protein Structure", which was part of the "Human Capital and Mobility Program". The experimental part of the work was carried out when C.L. was a graduate student in the laboratory of W.D at the University of Bremen. R.S.S. acknowledges support from the EPSCOR-NSF grant for "The Influence of Asymmetric and Non-Planar Distortions on Functional Properties of Metalloporphyrins in Solution and in Proteins" (PREPSCOR Grant OSR-9452893). Sandia is a multiprogram laboratory operated by Sandia Corporation, a Lockheed-Martin company, for the United States Department of Energy under Contract DE-AC04-94AL85000. We thank Esko Unger for many useful discussions with respect to the normal coordinate calculations.

Supporting Information Available: REPs and DPDs of all investigated Raman lines of Ni(5-NO_2−OEP) (Figures S1−S4) and Ni(5,15-diNO_2−OEP) (Figures S5−S8). This information is available free of charge via the internet at: http://pubs.acs.org.

Note Added after ASAP Posting. This article was posted ASAP without a description of the Supporting Information on 6/13/01. The correct version was posted on 6/22/01.

References and Notes

(1) Vicente, M. G. H. In *The Porphyrin Handbook. Vol. 1: Synthesis an Organic Chemistry*; Kadish, K. M., Smith, K. M., Guilard, R., Eds.; Academic Press: New York, 2000; pp 149−200.

(2) Senge, M. O. In *The Porphyrin Handbook. Vol. 1: Synthesis an Organic Chemistry*; Kadish, K. M., Smith, K. M., Guilard, R., Eds.; Academic Press: New York, 2000; pp 239−348.

(3) Shelnutt, J. A. In *The Porphyrin Handbook. Vol. 7: Theoretical and Physical Characterization*; Kadish, K. M., Smith, K. M., Guilard, R., Eds.; Academic Press: New York, 2000; pp 167−223.

(4) Jentzen, W.; Simpson, M. C.; Hobbs, J. D.; Song, X.; Ema, T.; Nelson, N. Y.; Medforth, C. J.; Smith, K. M.; Veyrat, M.; Mazzanti, M.; Ramasseul, R.; Marchon, J.-C.; Takeuchi, T.; Goddard, W. A., III; Shelnutt, J. A. *J. Am. Chem. Soc.* **1995**, *117*, 11085−11097.

(5) Song, X.-Z.; Jentzen, W.; Jia, S.-J.; Jaquinod, L.; Nurco, D. J.; Medforth, C. J.; Smith, K. M.; Shelnutt, J. A. *J. Am. Chem. Soc.* **1996**, *118*, 12975−12988.

(6) Duval, H.; Bulach, V.; Fischer, J.; Weiss, R. *Inorg. Chem.* **1999**, *38*, 5495−5501.

(7) Tsuchiya, S. *J. Am. Chem. Soc.* **1999**, *121*, 48−53.

(8) Senge, M. O.; Medforth, C. J.; Forsyth, T. P.; Lee, D. A.; Olmstead, M. M.; Jentzen, W.; Pandey, R. K.; Shelnutt, J. A.; Smith. K. M. *Inorg. Chem.* **1997**, *36*, 1149−1163.

(9) Anderson, K.; Hobbs, J. D.; Luo, L.; Stanley, K. D.; Quirke, J. M. E.; Shelnutt, J. A. *J. Am. Chem. Soc.* **1993**, *115*, 12346−12352.

(10) Hobbs, J. D.; Majumder, S. A.; Luo, L.; Sickelsmith, G. A.; Quirke, J. M. E.; Medforth, C. J.; Smith, K. M.; Shelnutt, J. A. *J. Am. Chem. Soc.* **1994**, *116*, 3261−3270.

(11) Chirvony, V. S.; van Hoeck, A.; Schaafsnab, T. J.; Pershukevich, P. P.; Filatov, I. V.; Avilov, I. V.; Shishporenok, S. I.; Terekhov, S. N.; Malinovskii, V. L. *J. Phys. Chem. B* **1998**, *102*, 9714−9724.

(12) Senge, M. *J. Porphyrins Phthalocyanines* **1998**, *2*, 107−121.

(13) Unger, E.; Beck, M.; Lipski, R. J.; Dreybrodt, W.; Medforth, C. J.; Smith, K. M.; Schweitzer-Stenner, R. *J. Phys. Chem. B* **1999**, *103*, 10022−10031.

(14) Schweitzer-Stenner, R.; Lemke, C.; Shelnutt, J. A.; Quirke, J. M. E.; Dreybrodt, W. *J. Phys. Chem. A* **2001**, *105*, 6680.

(15) Bonnet, R.; Stephenson, G. F. *J. Org. Chem.* **1965**, *30*, 2791.

(16) Unger, E.; Dreybrodt, W.; Schweitzer-Stenner, R. *J. Phys. Chem. A* **1997**, *101*, 5997−6007.

(17) Dreybrodt, W.; Jentzen, W.; Stichternath, A. In *Proceedings of the XIV-th Conference on Raman Spectroscopy*; Yu, N.-T., Li, X.-Y., Eds.; Wiley: Chichester, U.K., 1994; pp 1064−1065.

(18) Sato, S.; Kitagawa, T. *Appl. Phys. B* **1994**, *59*, 415−431.

(19) Unger, E.; Lipski, R. J.; Dreybrodt, W.; Schweitzer-Stenner, R. *J. Raman Spectrosc.* **1998**, *30*, 3−28.

(20) Herbstein, F. H.; Kapen, M. *Acta Crystallogr*. **1990**, *B46*, 567−574.

(21) Li, X.-Y.; Czernuszewicz, R.; Kincaid, J. R.; Stein, P. R.; Spiro, T. G. *J. Phys. Chem.* **1990**, *94*, 47−61.

(22) Stichternath, A.; Schweitzer-Stenner, R.; Dreybrodt, W.; Mak, R. S. W.; Li, X.-Y.; Sparks, L. D.; Shelnutt, J. A.; Medforth, C. J.; Smith, K. M. *J. Phys. Chem.* **1993**, *97*, 3701−3708.

(23) Piffat, C.; Melamed, S.; Spiro, T. G. *J. Phys. Chem.* **1993**, *97*, 7441−7449.

(24) Schweitzer-Stenner, R. *J. Porphyrins Phthalocyanines* **2001**, *5*, 198−224.

(25) Unger, E.; Bobinger, U.; Dreybrodt, W.; Schweitzer-Stenner, R. *J. Phys. Chem.* **1993**, *97*, 9956−9968.

(26) Jentzen, W.; Unger, E.; Karvounis, G.; Shelnutt, J. A.; Dreybrodt, W.; Schweitzer-Stenner, R. *J. Phys. Chem.* **1996**, *100*, 14184−14191.

(27) Franco, R.; Ma, J.-G.; Lu, Y.; Ferreira, G. C.; Shelnutt, J. A. *Biochemistry* **2000**, *39*, 2517−2529.

(28) Shelnutt, J. A.; Medforth, C. J.; Berber, M. D.; Barkigia, K. M.; Smith, K. M. *J. Am. Chem. Soc.* **1991**, *113*, 4077−4087.

(29) Spiro, T. G.; Li, X.-Y. In *Biological Application of Raman Spectroscopy*; Spiro, T. G., Ed.; Wiley: New York, 1988; pp 1−38.

(30) Shelnutt, J. A.; Majumder, S. A.; Sparks, L. D.; Hobbs, J. D.; Medforth, C. J.; Senge, M. O.; Smith, K. M.; Miura, M.; Luo, L.; Quirke, J. M. E. *J. Raman Spectrosc.* **1992**, *23*, 523.

(31) Franco, R.; Ma, J.-G.; Lu, Y.; Ferreira, G. C.; Shelnutt, J. A. *Biochemistry* **2000**, *39*, 2517.

(32) Unger, E. Ph.D. Thesis, Universität Bremen, Bremen, Germany, 1996.

(33) Gouterman, M. *J. Chem. Phys.* **1959**, *30*, 1139−1161.

(34) Lemke, C.; Dreybrodt, W.; Shelnutt, J. A.; Quirke, J. M. E.; Schweitzer-Stenner, R. *J. Raman Spectrosc.* **1998**, *29*, 945−953.

(35) Schweitzer-Stenner, R. *Q. Rev. Biophys.* **1989**, *22*, 381−479.

(36) Zhu, L.; Sage, J. T.; Champion, P. M. *Science* **1994**, *266*, 629−635.